Supporting Information

Gilchrist et al. 10.1073/pnas.1314557110

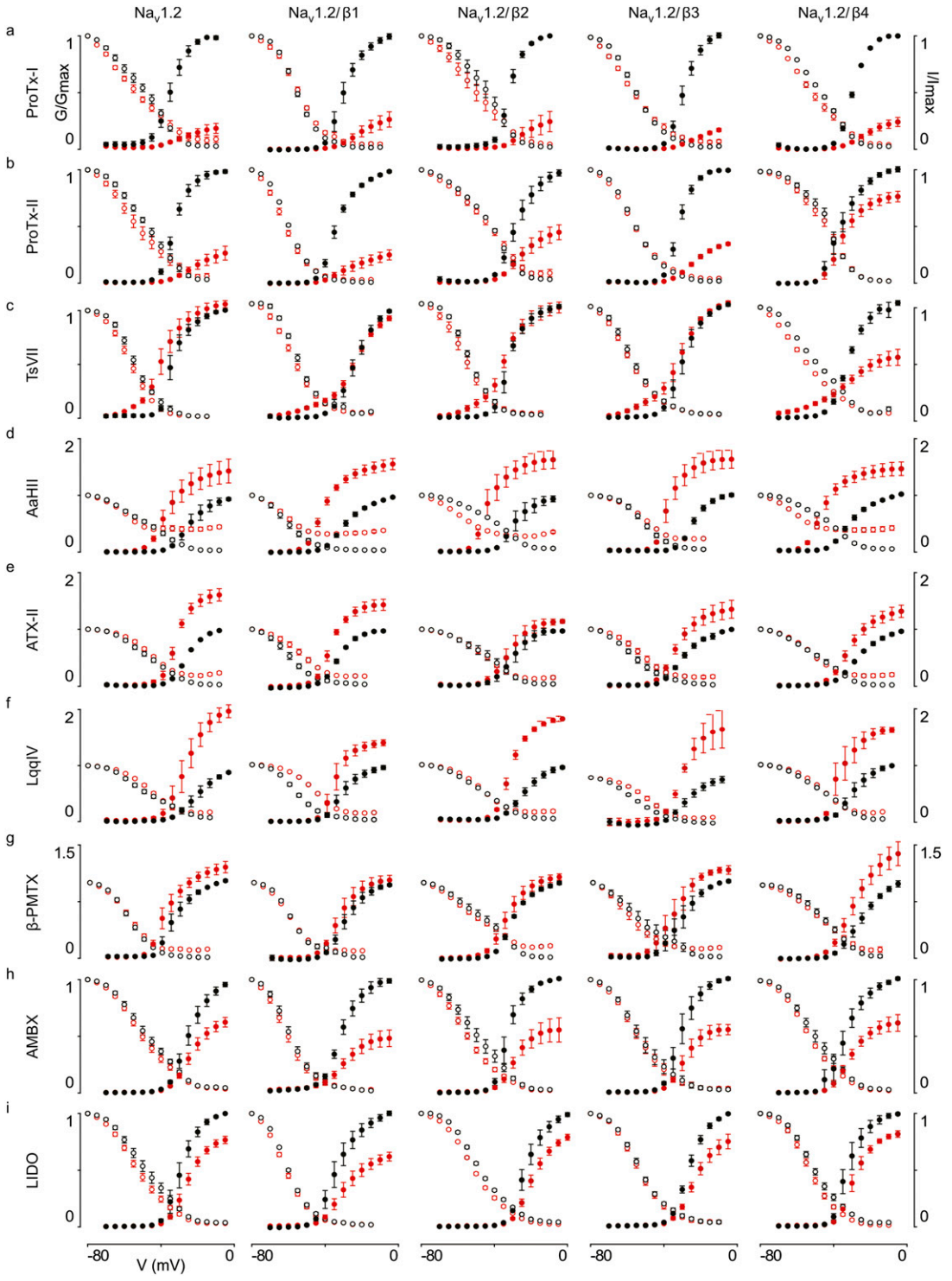

Fig. S1. Influence of β-subunits on the ligand susceptibility of the voltage-gated sodium channel Na$_v$1.2. Effect of 100 nM ProTx-I (*A*), 100 nM ProTx-II (*B*), 500 nM TsVII (*C*), 100 nM AaHII (*D*), 500 nM ATX-II (*E*), 100 nM LqqIV (*F*), 10 μM β-PMTX (*G*), 10 mM lidocaine (LIDO) (*H*), and 500 μM ambroxol (AMBX) (*I*) (all saturating concentrations) on Na$_v$1.2 without and in the presence of β-subunits. Normalized conductance–voltage relationships (G/G$_{max}$; black filled circle/red filled circle) and steady-state inactivation relationships (I/I$_{max}$; black open circle/red open circle) are shown before (black) and after (red) toxin or drug application. Channel-expressing oocytes were depolarized in 5-mV steps from a holding potential of −90 mV. n = 3–5; error bars represent S.E.M.

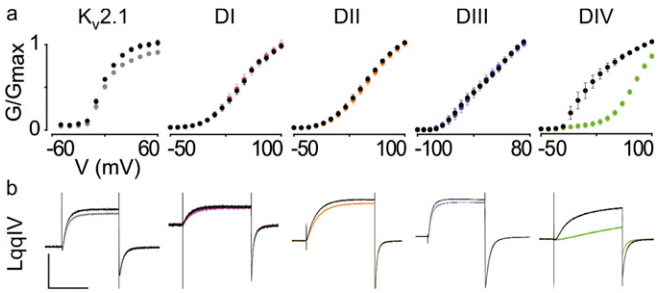

Fig. S2. Sensitivity of $Na_v1.2$ paddle chimaeras to LqqIV. (*A*) Effects of 100 nM LqqIV on voltage-gated potassium channel 2.1 ($K_v2.1$) and chimaeras in which paddle motifs from each of the four domains (DI–IV) were transferred from $Na_v1.2$ into $K_v2.1$ (1). Normalized tail current–voltage activation relationships are shown, with tail current amplitude plotted against test voltage before (black filled circles) and in the presence of (other colors) toxin. Data reveal that LqqIV selectively targets the paddle motif in DIV of $Na_v1.2$. The holding voltage was −90 mV, test pulse duration was 300 ms, and the tail voltage was −60 mV (−80 mV for DIII). (*B*) Potassium currents elicited by depolarizations near the foot of the voltage–activation curve for $K_v2.1$ and chimaeras in the absence and presence of 100 nM LqqIV. The *x*-axis is 100 ms; the *y*-axis is ∼0.5 μA.

1. Bosmans F, Martin-Eauclaire MF, Swartz KJ (2008) Deconstructing voltage sensor function and pharmacology in sodium channels. *Nature* 456(7219):202–208.

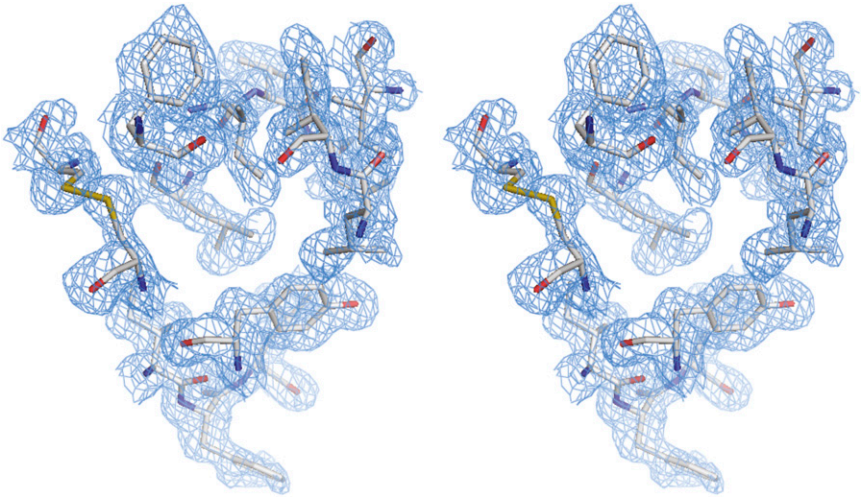

Fig. S3. Omit map of the β4 core. A stereo view of a simulated annealing composite omit map of the β4 subunit core contoured at 1σ. The ^{53}C–^{131}C disulfide bond (yellow) is present in this view.

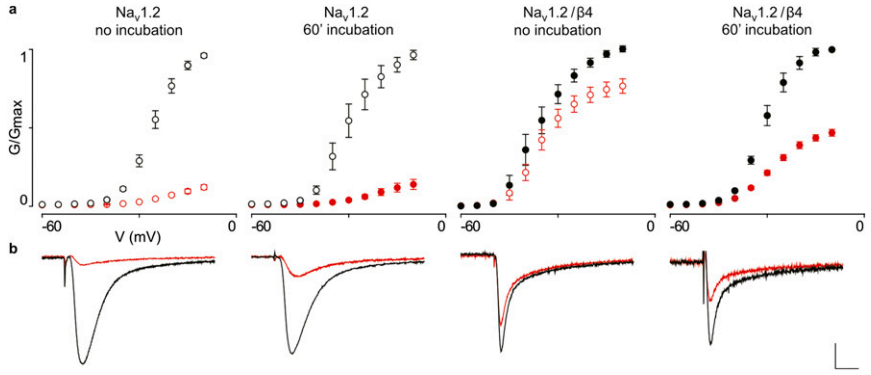

Fig. S4. Reducing ^{58}Cys abolishes the effect of β4 on ProTx-II binding. (*A*) Normalized conductance–voltage relationships (G/G_{max}) of $Na_v1.2$ and $Na_v1.2$/β4-expressing oocytes are shown before (black circles) and after (red circles) the application of 100 nM ProTx-II in control (no incubation; panels 1 and 3) and after 60 min incubation with 200 μM DTT and 100 μM EDTA (panels 2 and 4). As shown in this figure, $Na_v1.2$ opening is not significantly affected by the treatment; however, Cys reduction results in an increased affinity of ProTx-II for the Na_v channel in the presence of β4. Channel-expressing oocytes were depolarized in 5-mV steps from a holding potential of −90 mV. $n = 3$–5; error bars represent S.E.M. (*B*) Representative sodium currents are elicited by a depolarization to −20 mV before (black) and after (red) the addition of 100 nM ProTx-II from a holding potential of −90 mV. The *x*-axis is 10 ms; the *y*-axis is ∼0.5 μA.

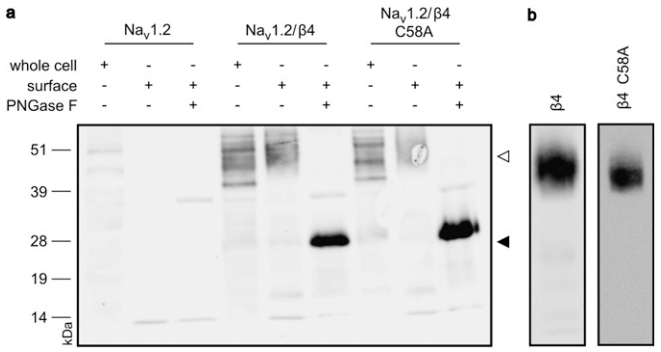

Fig. S5. β4 and the C58A mutant are glycosylated and traffic to the membrane. (*A*) Western blot analysis and biotinylation experiments demonstrate the presence of β4 and the C58A mutant on the oocyte membrane surface, albeit in a glycosylated form (open arrowhead). Removing β4 glycosylation using Peptide-*N*-Glycosidase F (PNGase F) incubation reveals the correct predicted molecular mass of 28 kDa (filled arrowhead).This figure shows data related to that shown in Fig. 4 but over a more extensive range of protein masses. (*B*) Without Na$_v$1.2, β4 (1) and the C58A mutant still traffic to the oocyte membrane in a glycosylated form. A ladder in kilodaltons (kDa) is shown on the left.

1. Yu FH, et al. (2003) Sodium channel beta4, a new disulfide-linked auxiliary subunit with similarity to beta2. *J Neurosci* 23(20):7577–7585.

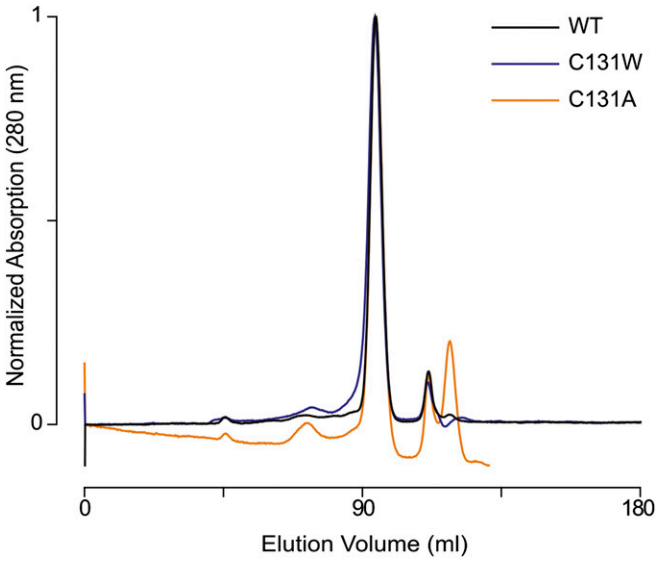

Fig. S6. Gel-filtration chromatograms of β4, C131W, and C131A. All three chromatograms display a predominant peak corresponding to monomeric protein. Normalized absorption was recorded at 280 nm.

Table S1. Influence of ligands on the gating properties of Na$_v$1.2 and Na$_v$1.2/βx

		Na$_v$1.2, mV		Na$_v$1.2/β1, mV		Na$_v$1.2/β2, mV		Na$_v$1.2/β3, mV		Na$_v$1.2/β4, mV	
Ligand	Parameter	Before	After	Before	After	Before	After	Before	After	Before	After
ProTx-I	Activation ($V_{1/2}$)	−34.2 ± 1.4	−28.0 ± 1.1*	−29.8 ± 1.5	−20.9 ± 0.2*	−31.8 ± 0.9	−22.5 ± 1.8*	−29.1 ± 1.4	−21.3 ± 0.9*	−29.3 ± 0.2	−22.8 ± 0.6*
	Inactivation ($V_{1/2}$)	−50.2 ± 1.7	−56.6 ± 1.4	−55.5 ± 0.6	−55.8 ± 1.0	−45.2 ± 2.6	−53.1 ± 4.3	−55.7 ± 0.7	−61.7 ± 0.7	−47.9 ± 0.3	−54.1 ± 0.9*
ProTx-II	Activation ($V_{1/2}$)	−32.3 ± 0.9	−22.5 ± 0.2*	−33.6 ± 0.9	−24.8 ± 3.0*	−27.7 ± 2.1	−24.6 ± 2.1	−31.7 ± 1.0	−24.0 ± 0.9*	−31.1 ± 3.3	−34.6 ± 3.4
	Inactivation ($V_{1/2}$)	−49.2 ± 1.3	−55.2 ± 2.5	−60.0 ± 0.3	−63.5 ± 1.0	−43.0 ± 0.3	−46.3 ± 1.3	−56.1 ± 0.5	−57.8 ± 0.2	−43.2 ± 0.9	−44.7 ± 1.5
TsVII	Activation ($V_{1/2}$)	−33.5 ± 1.5	−38.6 ± 2.1*	−23.0 ± 1.8	−23.4 ± 1.2	−32.0 ± 0.9	−35.0 ± 0.9	−29.6 ± 1.9	−31.1 ± 2.4	−31.0 ± 1.0	−33.0 ± 1.7
	Inactivation ($V_{1/2}$)	−54.3 ± 1.0	−56.9 ± 1.0	−55.4 ± 0.4	−58.1 ± 0.8	−53.7 ± 0.7	−56.8 ± 1.8	−57.6 ± 1.2	−59.8 ± 1.1	−51.8 ± 0.6	−59.4 ± 1.5*
LqqIV	Activation ($V_{1/2}$)	−18.5 ± 0.7	−24.4 ± 1.4*	−28.2 ± 1.7	−31.8 ± 1.8	−24.5 ± 1.5	−32.4 ± 0.8*	−28.4 ± 1.7	−32.3 ± 1.8	−30.0 ± 2.3	−37.2 ± 3.0
	Inactivation ($V_{1/2}$)	−50.5 ± 1.5	−48.0 ± 0.8	−56.8 ± 0.6	−48.1 ± 0.3*	−47.7 ± 0.5	−48.9 ± 0.6	−56.9 ± 1.0	−50.9 ± 1.0*	−47.3 ± 0.5	−48.0 ± 0.6
AMBX	Activation ($V_{1/2}$)	−24.4 ± 1.9	−23.3 ± 1.8	−30.5 ± 1.7	−29.2 ± 1.7	−32.8 ± 1.5	−29.5 ± 0.6	−30.4 ± 2.1	−28.4 ± 1.3	−34.1 ± 2.7	−31.2 ± 1.7
	Inactivation ($V_{1/2}$)	−49.1 ± 2.0	−51.5 ± 1.5	−60.0 ± 1.2	−61.9 ± 1.4	−50.7 ± 2.6	−57.4 ± 1.4	−54.3 ± 1.9	−55.4 ± 1.3	−50.7 ± 2.0	−54.2 ± 0.8

Results are the average of three to five oocyte recordings and errors are SEM. The table presents data related to Fig. 1 in the main text.
*A statistically significant difference before and after toxin addition to Na$_v$1.2 without or in the presence of a particular β-subunit (Student *t* test with $P < 0.005$).

Table S2. Disease mutations mapped onto the β4 structure

	Mutation (ref.)	Disease phenotype	Residue	Location	Solvent-accessible surface area, Å^{2†}
β1	R85H (1)	Atrial fibrillation	K96	End of β_5	61.9
	E87Q (2)	Cardiac conduction defect	D98	β_5– β_6 loop	21.4
	I106P (3)	Dravet syndrome	I116	β_7, within hydrophobic core	0.7
	C121W (4)	GEFS+	C131	β_8, affects conserved cysteine bond	0.9
	R125L (5)	GEFS+	N135	End of β_8, lines pocket next to ^{58}Cys.	14.3
	R125C (6)	Dravet syndrome	N135	End of β_8, lines pocket next to ^{58}Cys	14.3
	V138I (7)	Idiopathic epilepsy	—	Insertion in β_9–β_{10} loop	—
β3	V54G (8)	Idiopathic ventricular fibrillation	—	Insertion in β_2–β_3 loop	—
	Q89L (9)	Colorectal cancer*	D98	β_5-β_6 loop, surface accessible	21.4
	V110I (10)	Brugada syndrome	L121	β_7–3_{10} loop, within hydrophobic core	0

Although several β2 and β4 mutations have been implicated in atrial fibrillation and LQTS in humans, the amino acid substitutions involved occur outside of the crystal structure reported in this work and are not represented in this table. GEFS+: generalized epilepsy plus febrile seizures plus.

*Mutation found in a screen of colorectal cancer sample. The pathogenicity of the mutation has not been established, but the same position is also affected in a β1 mutation.

†Accessible surface area is for the side chain of the WT residue only.

1. Watanabe H, et al. (2009) Mutations in sodium channel β1- and β2-subunits associated with atrial fibrillation. *Circ Arrhythm Electrophysiol* 2(3):268–275.
2. Fendri-Kriaa N, et al. (2011) New mutation c.374C>T and a putative disease-associated haplotype within SCN1B gene in Tunisian families with febrile seizures. *Eur J Neurol* 18(5): 695–702.
3. Ishikawa T, et al. (2013) Novel SCN3B mutation associated with brugada syndrome affects intracellular trafficking and function of Nav1.5. *Circ J* 77(4):959–967.
4. Wallace RH, et al. (1998) Febrile seizures and generalized epilepsy associated with a mutation in the Na+-channel beta1 subunit gene SCN1B. *Nat Genet* 19(4):366–370.
5. Patino GA, et al. (2009) A functional null mutation of SCN1B in a patient with Dravet syndrome. *J Neurosci* 29(34):10764–10778.
6. Ogiwara I, et al. (2012) A homozygous mutation of voltage-gated sodium channel β(I) gene SCN1B in a patient with Dravet syndrome. *Epilepsia* 53(12):e200–e203.
7. Orrico A, et al. (2009) Mutational analysis of the SCN1A, SCN1B and GABRG2 genes in 150 Italian patients with idiopathic childhood epilepsies. *Clin Genet* 75(6):579–581.
8. Valdivia CR, et al. (2010) Loss-of-function mutation of the SCN3B-encoded sodium channel beta3 subunit associated with a case of idiopathic ventricular fibrillation. *Cardiovasc Res* 86(3):392–400.
9. Sjöblom T, et al. (2006) The consensus coding sequences of human breast and colorectal cancers. *Science* 314(5797):268–274.
10. Baroni D, Barbieri R, Picco C, Moran O (2013) Functional modulation of voltage-dependent sodium channel expression by wild type and mutated C121W-β1 subunit. *J Bioenerg Biomembr* 45(4):353–368.